Stimulation Pattern Efficiency in Percutaneous Auricular Vagus Nerve Stimulation: Experimental versus Numerical data

E. Kaniusas*, A.M. Samoudi, S. Kampusch, K. Bald, E. Tanghe, L. Martens, W. Joseph, and J. C. Széles

Abstract*— *Objective: **Percutaneous electrical stimulation of the auricular vagus nerve (pVNS) is an electroceutical technology. The selection of stimulation patterns is empirical, which may lead to under-stimulation or over-stimulation. The objective is to assess the efficiency of different stimulation patterns with respect to individual perception and to compare it with numerical data based on in-silico ear models.**

Methods: **Monophasic (MS), biphasic (BS) and triphasic stimulation (TS) patterns were tested in volunteers. Different clinically-relevant perception levels were assessed. In-silico models of the human ear were created with embedded fibers and vessels to assess different excitation levels.**

Results: **TS indicates experimental superiority over BS which is superior to MS while reaching different perception levels. TS requires about 57% and 35% of BS and MS magnitude, respectively, to reach the comfortable perception. Experimental thresholds are decreased from bursted to non-bursted stimulation. Numerical results indicate a slight superiority of BS and TS over MS while reaching different excitation levels, whereas the burst length has no influence. TS yields the highest number of asynchronous action impulses per stimulation symbol for the used tripolar electrode set-up.**

Conclusion: **The comparison of experimental and numerical data favors the novel TS pattern. The analysis separates excitatory pVNS effects in the auricular periphery, as accounted by in-silico data, from the combination of peripheral and central pVNS effects in the brain, as accounted by experimental data.**

Significance: **The proposed approach moves from an empirical selection of stimulation patterns towards efficient and optimized pVNS settings.**

***Index Terms*—auricular nerves, in-silico modeling, personalized stimulation, stimulation optimization, stimulation patterns, vagus nerve stimulation.**

*E. Kaniusas is with the Institute of Electrodynamics, Microwave and Circuit Engineering, Vienna University of Technology, Vienna, Austria (correspondence e-mail: kaniusas@tuwien.ac.at).

S. Kampusch and K. Bald are with the Institute of Electrodynamics, Microwave and Circuit Engineering, Vienna University of Technology, Vienna, Austria. A.M. Samoudi, E. Tanghe, L. Martens, and W. Joseph are with the Department of Information Technology, Ghent University/IMEC, Ghent, Belgium. J.C. Széles is with the Department of Surgery, Medical University of Vienna, Vienna, Austria.

I. Introduction

ELECTRICAL vagus nerve stimulation progressively comes into focus as a significant part of bioelectronic medicine for non-pharmacological treatment of various diseases [1], [2], [3]. Here the percutaneous electrical stimulation of the auricular vagus nerve (pVNS) using miniature needles within the vagally innervated regions of the ear [4] gained a special interest [5]. In addition, methods for transcutaneous stimulation of the auricular vagus nerve via surface electrodes [3] and for invasive stimulation of the cervical branch of vagus nerve via implanted electrodes [6] are available. pVNS avoids diffuse stimulation of auricular nerve endings and implantation risks of transcutaneous and invasive approaches, respectively [5], as summarized in our recent review [7].

Stimulation of the afferent vagus nerve modulates sensorial input to the brain. It changes activation patterns of specific brain structures, especially of the nucleus of the solitary tract in the brainstem, and thus modulates the parasympathetic part of the autonomic nervous system with its systemic effects affecting the whole body. pVNS can be expected to be mostly sympatho-inhibitory in origin [8], [9].

In particular - as recently reviewed by our group [10] - auricular stimulation seems to alter signal processing and reflex circuitries in the brain [11], [12]. The vagal stimulation, in general, modulates nociceptive processing [13] and inflammation [14], as well as serotonergic, noradrenergic, and endorphinergic pathways in the brain [15]. Diverse systemic physiological parameters are affected such as heart rate variability [8], [16], [17], peripheral blood perfusion [18], and sympathetic outflow [19]. pVNS is targeted in chronic pain syndromes [20], [21], neurological, neurodegenerative, and metabolic ailments [22], [23], [24] as well as inflammatory and cardiovascular diseases [2], [25].

Different devices have been used for clinical investigations of auricular vagus nerve stimulation [19], [20], [26], [27]. The used stimulation settings differ from one device to another and are based on empirical observations [5]. Even though the stimulation magnitude is individually adjusted in some devices, optimal stimulation patterns for pVNS are still undetermined. Thus, a suboptimal pVNS therapy can be expected to deliver suboptimal therapeutic results, leading

potentially to under-stimulation or over-stimulation.

For instance, for the transcutaneous auricular vagus nerve stimulation, authors in [28] show that different stimulation parameters yield different responses in the heart rate, whereas authors in [29] use vagus somatosensory evoked potentials to optimize parameters. The physiological and therapeutic relevance of the selected stimulation parameters, especially bursted versus non-bursted, is highlighted in [5], [30], [31], [32], [33].

However, the common denominator in used pVNS stimulation settings is that stimuli of a subjectively comfortable intensity are preferred to reach therapeutic targets [21], [34], whereas perception is a strong function of the stimulation pattern [35]. A tingling perception is necessary [3], [36] since the non-nociceptive pVNS should recruit myelinated Aβ fibers [37] of the auricular vagus nerve, which are responsible for cutaneous mechanoreception and touch sensation. pVNS should avoid pain perception and thus avoid stimulation of myelinated Aδ fibers of the auricular vagus nerve, devoted to cutaneous pain and temperature sensation. Authors in [13] suggest that non-painful innocuous peripheral nerve stimulation preferentially activates Aβ fibers but not Aδ nociceptive fibers in the ear. As a practical advantage for pVNS, relatively thick Aβ fibers (with the diameter 7-10μm) can be easier recruited than relatively thin Aδ fibers (2-5μm).

This association between subjective perception and recruitment of auricular Aβ and/or Aδ fibers warrants an optimisation of experimental perception and numerical simulation with respect to different stimulation patterns, as targeted by the present study. Namely, experimental thresholds of subjective comfortable perception are assumed to model mechanoreceptive and touch sensation of the ear, and thus are assumed to be related with numerical thresholds of the required Aβ excitation within proposed in-silico ear models. In contrast, experimental thresholds of subjective painful perception are assumed to model pain sensation of the ear and thus are assumed to be related with numerical thresholds of Aδ excitation.

In this paper, the perceptional efficiency of different stimulation patterns with respect to different modalities is - for the first time - compared and contrasted with numerical counterparts using powerful in-silico models. This work should offer useful insights into the experimental and numerical relevance of the stimulus waveform, shape, and burst lengths in pVNS.

II. Methods

A. Experimental Data

A pre-clinical single-blinded pilot study was carried out at the Medical University of Vienna on the systemic evaluation of stimulation parameters of pVNS. The study was approved by the local ethics committee (Nr. 1924/2013) and the Austrian Agency for Health and Food Safety, and was registered at ClinicalTrials.gov (NCT02098447). Ethical guidelines were implemented including detailed information and signed informed consent of all study participants.

The present study includes data on eight healthy adult volunteers without any pain (five females) aged 44 ± 13 years with body mass index 22 ± 4 kg/m^2. Three volunteers were of

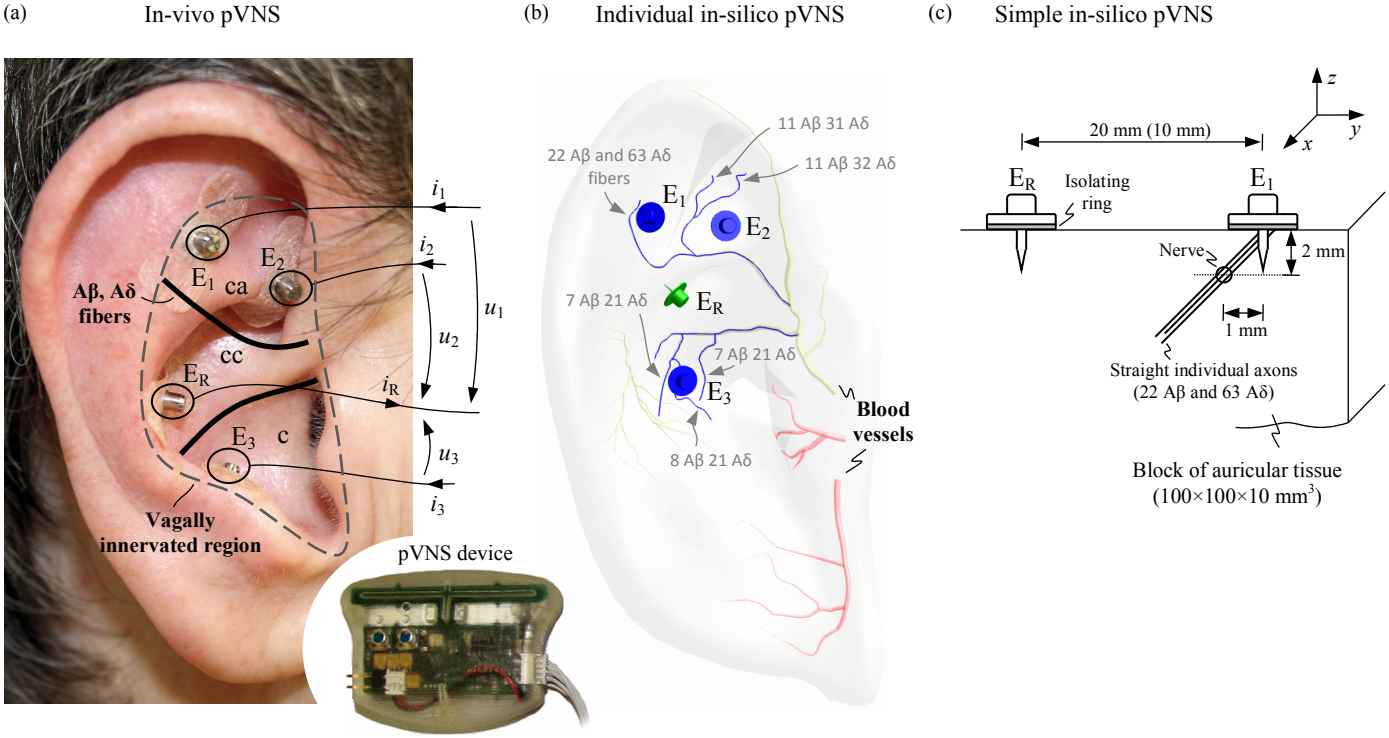

Fig. 1 In-vivo and in-silico models for the percutaneous auricular vagus nerve stimulation (pVNS). a) Ear with vagally innervated regions and four percutaneous needle electrodes: three stimulation electrodes (E_1 to E_3) and a reference electrode (E_R). b) Individual in-silico model for pVNS composed out of individually-wired auricular blood vessels (yellow and red), two auricular vagus nerve branches running along vessels (blue), and needle electrodes $E_{1..3}$ (blue) and E_R (green). c) Simple in-silico model for pVNS composed out of a tissue block with an embedded single nerve and two stimulation electrodes E_1 and E_R.

age < 40 (two females). As shown in Fig. 1a, four stimulation needles with the penetration depth of 2mm were placed in the ear, namely, three active needle electrodes (E_1 to E_3) and one reference needle electrode (E_R). Here auricular regions were selected which are partly or solely innervated by the vagus nerve: cymba conchae (cc), cavity of conchae (c), and crura of antihelix (ca) [4]. Needles were positioned close to vessel-nerve bundles, as located by measuring the local resistance of the auricle (Multi-Point from Biegler Medizinelektronik GmbH, Austria) and by visual inspection of the auricular vessel structure. Needle electrodes were wired with the voltage-controlled output of a proprietary portable µC-based stimulator (Fig. 1a) - build by the Vienna University of Technology, for technical characteristics see row IV in Table I [38] - that is battery powered and wirelessly controlled. The capacitive coupling between electrodes and the stimulator output avoided electric charge imbalance at the electrode/tissue boundary and thus irreversible electrochemical reactions over time.

The applied stimulation patterns of the voltage $u_1(t)$ to $u_3(t)$ on the active electrodes E_1 to E_3, respectively, with respect to E_R are illustrated in Fig. 2, with the burst repetition rate f_S of 1Hz and the peak amplitude U. Monophasic stimulation (MS) comprises a rectangular voltage pulse of 1ms duration t_P with zero voltage for the subsequent 1 ms, forming a single MS symbol with 2 ms duration (Fig. 2a). Here the pulse changes its polarity after each stimulation period $1/f_S$. Biphasic stimulation (BS) is formed out of consecutive up and down pulses each with $t_P = 1$ ms (Fig. 2b), forming a single BS symbol with 2 ms duration. A novel stimulation pattern, triphasic stimulation (TS), is composed out of six consecutive pulses of $t_P = 1$ms duration each, with the total duration of 6 ms of a single TS symbol (Fig. 2c). In TS, the sum over all three stimulation patterns $u_1(t)$ to $u_3(t)$ equals to zero voltage at any time, favorably unloading the resulting current i_R along the reference electrode (Fig. 1a). A variable burst length BL of 1, 30, or 250 symbols per second were implemented for MS and BS, with the respective total burst duration of 2 ms, 60 ms, and 500 ms. TS was tested with $BL = 1$, 15, or 125 symbols per second, with the respective total burst duration of 6 ms, 90 ms, and 750 ms. While the sequence of BS or TS symbols (for $BL > 1$) does not change from one burst to the next with the repetition rate f_S (Fig. 2b,c), the sequence of cathodic MS symbols ($BL > 1$) follows that of anodic MS symbols and vice versa in MS (Fig. 2a).

Three recording sessions were performed per study participant, with one measurement session per day on three consecutive days (reducing accommodation effects) in a quiet room and sitting position. Measurement sessions were initiated 1-2min after placement of needle electrodes. After each session, needles were removed. The stimulation side was switched from right to left ear (or vice versa) from one measurement session to the next. The electrode position was slightly altered from the first to third session - when the same ear was used - in order to avoid both formation of scar tissue and increase in the electrode impedance.

Each measurement session included nine tests (three stimulation patterns with the respective three different BL), with in total 27 tests per subject and 216 tests for the whole study. In each test, U of the selected stimulation pattern and BL was increased from 0V in small steps of 50 to 100 mV every 10 s until a particular individual perception level (PL) is reached. There was a short pause of at least 2 min in-between tests to avoid refractory behaviour. Single blinded tests were performed, i.e., subjects were not informed about the onset of the stimulation, the type and BL of the stimulation pattern, as well as about the applied change in U.

The first measurement session included the following tests (in chronological order): MS with $BL = 1$, 30, and 250, then BS with $BL = 1$, 30, and 250, and then TS with $BL = 1$, 15, 125. The second session started with BS with $BL = 1$, 30, and 250, then TS with $BL = 1$, 15, and 125, and then MS with $BL = 1$, 30, 250. The third session began with TS with $BL = 1$, 15, and 125, then MS with $BL = 1$, 30, 250, and then BS with

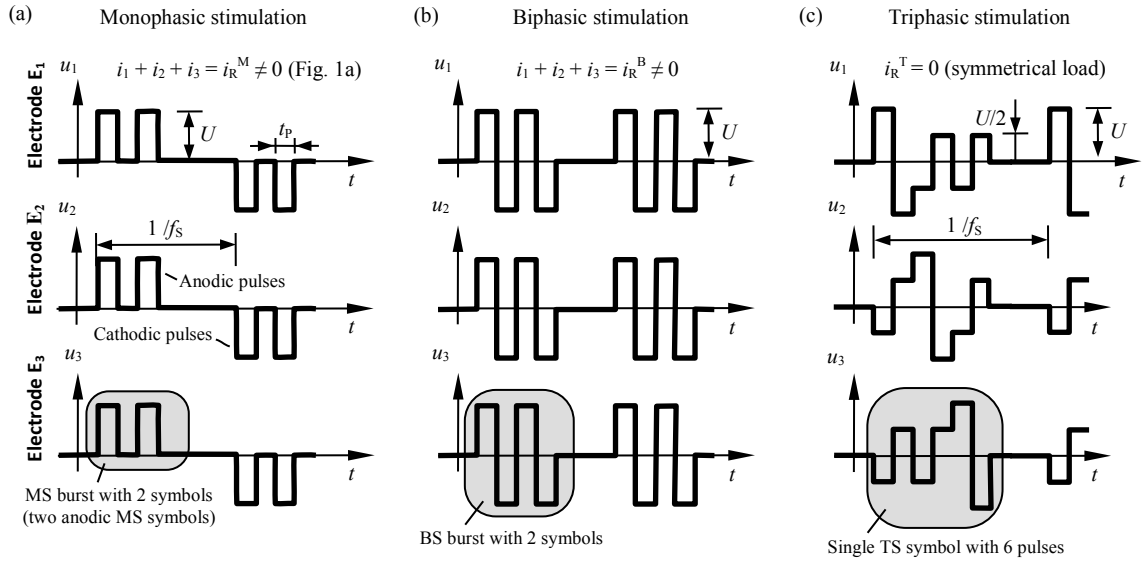

Fig. 2 Stimulation patterns of the voltage applied on electrodes E_1 to E_3 (Fig. 1). a) Monophasic stimulation (MS) with the burst repetition rate f_S (= 1Hz), pulse duration t_P (= 1ms), and burst length BL (= 2). b) Biphasic stimulation (BS) with $BL = 2$. c) Triphasic stimulation (TS) with $BL = 1$.

BL = 1, 30, and 250.

For each test, three PLs of *U* were experimentally assessed: first the threshold perception (PLa), then the comfortable perception (PLb), and lastly the painful up to intolerable perception (PLc). All PLs were assessed as a function of the stimulation pattern and *BL*. At the end of each test, subjects reported verbally their subjective perception of the stimulation.

Values of *U* were averaged over all three measurement sessions for a given subject, PL, stimulation pattern, and *BL*. In order to assess the energetic footprint of the different stimulation patterns and the associated metabolic stress on auricular nerves, the effective value U_{eff}

$$U_{\mathrm{eff}}^2 = f_{\mathrm{S}} \cdot \int u^2(t)\,\mathrm{d}t \tag{1}$$

was calculated. For MS, BS, and TS, Eq. 1 yields the respective $U_{\mathrm{eff,MS}}$, $U_{\mathrm{eff,BS}}$, and $U_{\mathrm{eff,TS}}$ according to Fig. 2 given by

$$U_{\mathrm{eff,MS}} = \sqrt{f_{\mathrm{S}} \cdot U^2 \cdot t_{\mathrm{P}} \cdot BL}\ ,$$

$$U_{\mathrm{eff,BS}} = \sqrt{f_{\mathrm{S}} \cdot U^2 \cdot t_{\mathrm{P}} \cdot BL \cdot 2}\ \text{, and}$$

$$U_{\mathrm{eff,TS}} = \sqrt{f_{\mathrm{S}} \cdot U^2 \cdot t_{\mathrm{P}} \cdot BL \cdot 3}\ , \tag{2}$$

with *U* as the peak value, t_{P} the pulse duration, f_{S} the repetition rate, and *BL* the burst length. In a generalized form, Eq. 2 can be rewritten as

$$U_{\mathrm{eff}} = U \cdot \sqrt{t_{\mathrm{P}} \cdot f_{\mathrm{S}} \cdot BL} \cdot k \tag{3}$$

with $k = 1$ for MS, $k = \sqrt{2}$ for BS, and $k = \sqrt{3}$ for TS.

Data was tested for normal distribution using Kolmogorov-Smirnov test. Since data was not normally distributed, statistical differences between sample medians (between the different stimulation patterns and *BL*) within a single group of subjects were tested by the two-sided Wilcoxon signed rank test for paired dependent samples. Statistical differences between medians of different groups of subjects (between male and female, as well as age < 40 years versus age ≥ 40 years) were tested by the two-sided Wilcoxon rank sum test for two independent samples. An error probability of 0.05 was assumed for rejecting the null hypothesis (medians are equal) and the rejection is denoted by asterisks "*" (Fig. 3 to Fig. 5). All boxplots reflect the 25th, 50th (median), and 75th percentiles with whiskers extending to 1.5 of the interquartile range below the first quartile and above the third quartile (compare Fig. 3).

B. Numerical Data

Numerical simulation of pVNS requires a step-wise coupled electromagnetic and electrophysiological modelling, which was performed in the Sim4Life platform (from Zurich MedTech AG, Switzerland) [39]. First, the distribution of the electric field in the auricular tissue was calculated in response to the spatially distributed application of voltages $u_1(t)$ to $u_3(t)$ (Fig. 1a), using the low-frequency solver in Sim4Life. As in the experimental setting, $u_1(t)$ to $u_3(t)$ reflected the temporal stimulation patterns MS, BS, and TS with the variable *BL* (Fig. 2). The resulting distribution of the electric field considered the particular anatomy of the ear and the heterogeneity of local electrical properties - especially of the electrical conductivity - of the auricular tissue due to embedded blood vessels but without auricular nerves [40] (Fig. 1b). Here the auricular tissue conductivity was set to 0.2 S/m while that of embedded vessels to 0.7 S/m, in line with our recent works [41], [42].

Second, the resulting local electric fields in the auricle, their gradients and dynamics - along extracellular spaces of now embedded auricular axons and their endings - were used for the neural simulation, i.e., for excitation of axonal membranes. The dynamics of these electric fields were tightly connected with the temporal characteristics of $u_1(t)$ to $u_3(t)$ (Fig. 2). Here the physiological distribution density of fiber types in the ear, fiber trajectories, and their diameters as well as realistic fiber models were required, as these properties determine the physical stimulation depth and numerical thresholds of pVNS for specific electrode placement and stimulation waveform. Fig. 1b,c show the used models: a realistic and a simple in-silico model. We simulated auricular myelinated fibers and thus their transmembrane mechanisms with the SENN model [32] and the Sweeney model [43], both models being used and validated in Sim4Life. Titration mechanisms were used to find thresholds of excitation for single fibers. For more details on the low-frequency solver and neuronal modelling, the reader is referred to [41].

The realistic individual in-silico model is shown in Fig. 1b and has a spatial resolution of 3mm, including major auricular arteries (originating from the superficial temporal artery and the posterior auricular artery, colored in yellow and red in Fig. 1b), and two branches of the auricular vagus nerve (marked in blue in Fig. 1b). Branches and sub-branches of this modelled nerve are running alongside blood vessels since fibers and vessels are usually wired together, often alongside one another [44], even in the auricle [7], [40]. Nerves are modelled as bundles of fibers with a physical volume (given by the fiber diameter, see below) and conductivity (of 1 S/m [32]). A distance equal to the diameter of a single fiber is kept between two adjacent axons to simulate a dense population of axons [42].

Approximate locations of vessels and nerve branches in Fig. 1b are based on the vascularization of the auricle and the nerve supply of the human ear [4], [45], [46]. However, detailed distribution of vessels and nerves is highly individual; thus, a typical and exemplary distribution is selected in Fig. 1b. Vessels and nerve branches are located at least 70 µm under the skin surface, i.e., below the epidermal thickness at the thinnest parts of the human body [47]. In close agreement with the experimental setting (Fig. 1a), four stimulation electrodes E_1 to E_3 and E_R are located in vagally innervated regions of the

ear (regions cc, c, and ca from Fig. 1a) with their penetration depth of 2 mm (Fig. 1c).

The two branches of the modelled auricular vagus nerve in Fig. 1b are composed out of 66 myelinated thick Aβ fibers and 189 myelinated thin Aδ fibers, in agreement with numerical counts of dissected auricular axons [37]. Modelled Aβ fibers have the diameter 8.3 µm (their typical diameter is in the range 7-10 µm with the estimated average diameter 8.3 µm in the ear [37]), whereas Aδ fibers have the diameter 3.5 µm (with their typical diameter 2-5 µm and the estimated average 3.5 µm [37]). As shown in Fig. 1b, Aβ and Aδ fibers are distributed in a way that each active electrode E_1 to E_3 is surrounded by 1/3 of all Aβ and Aδ fibers, namely, by 22 Aβ and 63 Aδ fibers. These fibers reside relatively close to the respective needle electrodes, where they can be recruited due to the resulting high local electric fields and their high local gradients (around E_1 to E_3 in Fig. 7a). Particular numbers of embedded Aβ and Aδ fibers along splitting nerve branches are listed in Fig. 1b. A space equal to the diameter of a single axon is modelled between two adjacent axons to simulate a dense axon population [42].

In addition, a simple in-silico model for pVNS was established, as shown in Fig. 1c. The model provides comparative numerical data on pVNS since it excludes potential influence of individual geometrical, vascularization, and innervation features of the individual in-silico model (Fig. 1b). This simple model is a block of auricular tissue (100×100×10 mm^3) without vessels and with a single embedded straight-line nerve in the depth of 2 mm. A single stimulation electrode E_1 is pierced down to 2 mm into this block at a lateral distance of 1 mm from the nerve (Fig. 1c), whereas the reference electrode E_R is placed in a distance of 20 mm (or 10 mm for sensitivity analysis of the model, see the discussion section). This lateral distance was selected because needle electrodes are typically positioned in a distance of about 1 mm from identified auricular vessels in clinical pVNS applications to minimize risks of local bleeding. In line with the individual model, the nerve is composed out of 22 Aβ and 63 Aδ fibers for this single electrode E_1. The auricular block was positioned in the center of another larger block of air as the background domain (1000×1000×1000 mm^3), whose all six surfaces were subjected to the zero electric field (Neumann boundary condition). This distant setting of boundary conditions allows unrestricted distributions of the electric and current density fields within the auricular block.

For both models, three excitation levels (EL) of *U* were numerically assessed: the excitation threshold (ELa) of any single Aβ fiber in the ear during a single stimulation period $1/f_s$, the mechanoreceptive threshold (ELb) with at least a singular excitation of all modelled Aβ fibers during the period $1/f_s$, and the pain threshold (ELc) with at least a singular excitation of at least 50% of all modelled Aδ fibers within $1/f_s$. Thus, ELb and ELc were assessed as a function of the stimulation pattern and *BL*.

For both models, the total number *TN* of action impulses was counted for ELb and ELc within the single period $1/f_s$, and was related to the total number of the embedded Aβ and Aδ fibers (255 for the individual model and 85 for the simple model). Synchronous impulses at all electrodes (e.g., for MS or BS) as well as asynchronous impulses (for TS) individually contributed to *TN* regardless of their potential overlap in time. In approximation, *TN* provides the amount of sensorial information leaving the ear towards the brain. For instance, if we assume a single action impulse in response to every symbol in MS, BS, or TS (Fig. 6a,c), the expected calculated *TN* for the individual or simple model approximates 0.26 (= 66/255 = 22/85) for MS, *BL* = 1, and ELb. For ELc, we assume that all Aβ fibers become co-excited so that *TN* approximates 19 (= 30·(66+95)/255 ≈ 30·(22+32)/85) for BS and *BL* = 30; see Table 3 for the respective calculated *TN*.

Please note that for MS with its subsequent cathodic and anodic pulses (Fig. 2a), the simulated cathodic pulse of MS

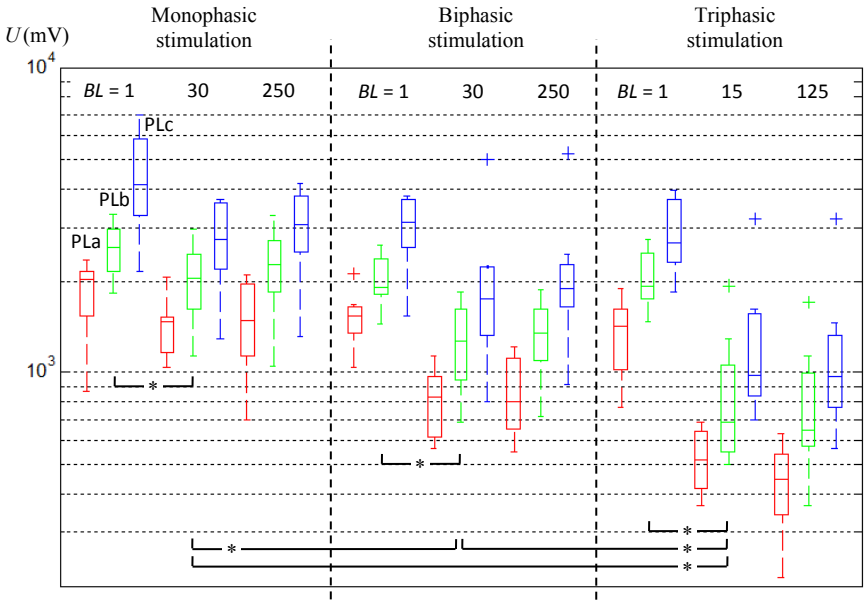

Fig. 3 In-vivo pVNS. Absolute peak amplitudes *U* of all perception levels PLa, PLb, and PLc, all burst durations *BL*, and all three different stimulation patterns.

TABLE 1
IN-VIVO PVNS. EXPERIMENTAL MEDIAN THRESHOLDS OF PEAK VALUES *U* ARE PROVIDED IN %, AS RELATED TO THE THRESHOLD PERCEPTION (PLA) AT THE MONOPHASIC STIMULATION (MS) WITHOUT BURSTING (*BL* = 1).

Burst length *BL*	Perception level PL	Monophasic stimulation MS (%)	Biphasic stimulation BS (%)	Triphasic stimulation TS (%)
1 for MS, BS, TS	PLb	139	107	106
	PLc	202	164	146
30 for MS, BS 15 for TS	PLb	101	62	36
	PLc	138	86	52
250 for MS, BS 125 for TS	PLb	109	66	38
	PLc	143	91	49

(Fig. 6a) was considered as being representative for the whole MS cycle in terms of the calculated EL-related levels of *U* and the resulting size of *TN*. This is because cathodic pulses typically show lower excitation thresholds than anodic pulses in extracellular stimulation [48].

III. RESULTS

A. Experimental Data

Experimental peak values *U* are shown in Fig. 3 as a function of the stimulation pattern, PL, and *BL*, whereas Table 1 provides the associated medians in % as related to PLa of each person of MS with *BL* = 1. No obvious differences in *U* were observed between all three measurement sessions for a given subject, PL, stimulation pattern, and *BL* (data not shown), which justified the averaging procedure over sessions.

In all tests, the registered *U* increases from PLa, to PLb and then to PLc, as expected from the experimental protocol. The bursted stimulation with *BL* > 1 decreases *U* to reach different PL when compared with the non-bursted stimulation with *BL* = 1. For instance, *U* of MS, BS and TS with *BL* of 30, 30 and 15 requires significantly lower levels of only about 73% (= 101/139), 58%, and 34% of *U* of MS, BS, and TS with *BL* = 1, respectively, to reach PLb (Table 1 and Fig. 3). A further increase of the duration of bursts seems to have no effects, e.g., *U* of MS, BS and TS with the respective *BL* of 250, 250 and 125 requires about 108%, 106%, and 106% (all non-significant) to reach PLb as compared with the respective *BL* of 30, 30 and 15 (Table 1).

For all PL and the non-bursted stimulation with *BL* = 1, *U* tends to decrease non-significantly from MS to BS or to TS. In contrast, for all PL and the bursted stimulation with *BL* > 1, *U* decreases significantly from MS to BS and then even further to TS. The smallest *U* is observed for PLa, TS with *BL* = 125, whereas the highest *U* for PLc, MS with *BL* = 1. For instance, in order to reach PLb for *BL* > 1, TS requires significantly lower magnitudes of only about 57% and 35% of BS and MS magnitude, respectively, whereas BS requires about 61% of MS magnitude (Table 1 and Fig. 3).

In line with (3), the derived effective U_{eff} in Fig. 4 yields identical tendencies as *U* (Fig. 3) with respect to changing PL for the given stimulation pattern and *BL*. In contrast, the

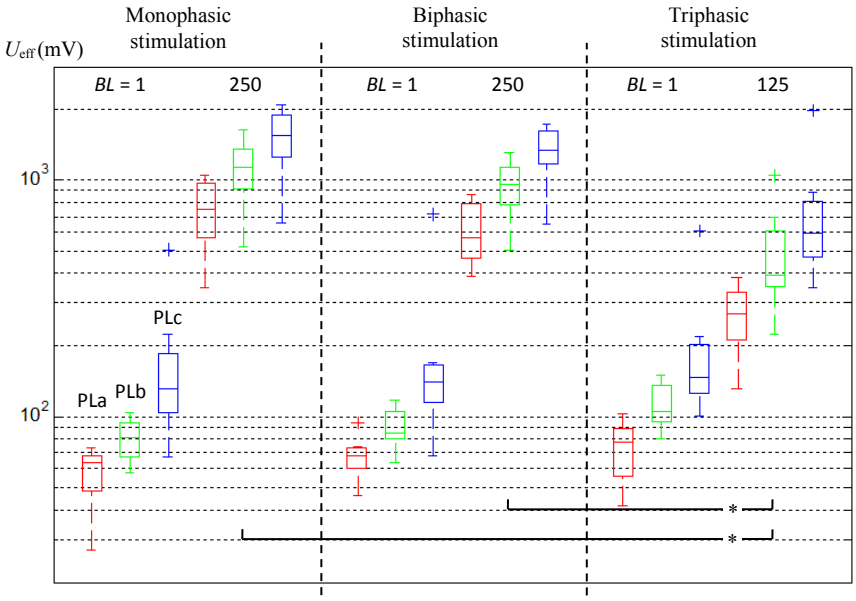

Fig. 4 In-vivo pVNS. Effective amplitudes U_{eff} of all perception levels PLa, PLb, and PLc, burst durations *BL* of 1 and 250, and different stimulation patterns.

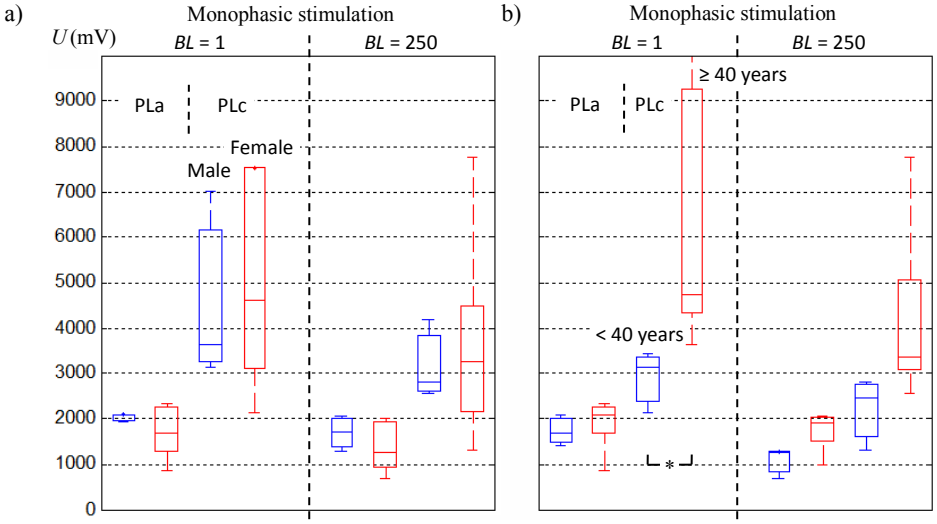

Fig. 5 In-vivo pVNS. Absolute peak amplitudes U of two perception levels PLa and PLc for burst lengths BL = 1 and 250 of monophasic stimulation. a) Male versus female. b) Age differences.

differences in U_{eff} between $BL = 1$ and $BL > 1$ become even reversed in comparison with those in U due to weighting effects of the square root of BL in (3), i.e., U_{eff} disproportionately increases with increasing BL for a given U.

From an energetic point of view and for a single symbol, MS is the most efficient set-up (with $k = 1$ in (3)), followed by BS ($k = 1.4$) and then by TS ($k = 1.7$). Therefore, the observed potential advantage of TS over BS and BS over MS in terms of the reduced U for $BL > 1$ is counterbalanced by this factor k; compare Fig. 3 for U and Fig. 4 for U_{eff}. However, TS with $BL > 1$ still seems to be superior to MS and BS with $BL > 1$ in terms of a significantly lowered U_{eff} (Fig. 4), considering not only perceptional aspects (PL-related) but also energetic aspects (k-related).

Males tend to show an insignificantly higher U than females for PLa and PLb, as applicable only for MS irrespective of BL (Fig. 5a). In contrast, females tend to reach an insignificantly higher U than males for PLc, irrespective of the stimulation pattern and BL. Fig. 5a compares U of PLa and PLc of males versus females for MS with BL of 1 and 250. For instance, males required 118%, 111%, and 79% of U of MS for PLa, PLb, and PLc in comparison with females, respectively (% values were calculated when averaging over all BL due to small sample size). All differences were non-significant.

Subjects of age < 40 tend to show a lower U than that of age ≥ 40 for all stimulation patterns irrespective of BL, with the largest difference for PLc. Fig. 5b compares U of PLa and PLc of age < 40 versus age ≥ 40 for MS with BL of 1 and 250, with the significant difference for $BL = 1$ and PLc only. For instance, subjects of age < 40 required 74%, 67%, and 47% of U of MS for PLa, PLb, and PLc in comparison with age ≥ 40, respectively; for TS the respective values were 92%, 66%, and 53% (all % values were calculated when averaging over all BL).

Volunteers described the non-bursted pVNS ($BL = 1$) as knocking and twitching, with the tendency to become uncomfortable soon. The bursted pVNS ($BL > 1$) was described as creeping and twitching, tingling and vibrating,

TABLE 2
SIMPLE AND INDIVIDUAL IN-SILICO PVNS. NUMERICAL THRESHOLDS OF PEAK VALUES U ARE PROVIDED IN %, AS RELATED TO THE MONOPHASIC CATHODIC STIMULATION (MS) WITHOUT BURSTING ($BL = 1$) LEADING TO EXCITATION OF AT LEAST A SINGLE Aβ FIBER. TWO DIFFERENT NUMERICAL FIBER MODELS ARE CONSIDERED (SWEENEY/SENN). IN CONTRAST TO EXPERIMENTAL DATA (TABLE 1), NUMERICAL THRESHOLDS TURNED OUT TO BE INDEPENDENT ON BL.

	Excitation level EL	Monophasic stimulation MS (%)	Biphasic stimulation BS (%)	Triphasic stimulation TS (%)
Simple in-silico pVNS	ELb	117.3 / 117.9 (119.4 / 118.2)*	112.3 / 117.2 (114.0 / 116.9)*	112.3 / 117.2 (114.0 / 116.9)*
	ELc	310.8 / 287.6 (311.0 / 285.7)*	232.2 / 220.8 (238.4 / 223.4)*	232.2 / 220.8 (238.4 / 223.4)*
Individual in-silico pVNS	ELb	182.5 / 180	174.7 / 178.9	174.7 / 178.9
	ELc	254.3 / 235.5	244.6 / 235.5	244.6 / 235.5

* For comparison, threshold values are provided for the halved distance of 10 mm (= 20 mm / 2) between the reference electrode E_R and active electrode E_1 (Fig. 1c) for the simple in-silico pVNS model.

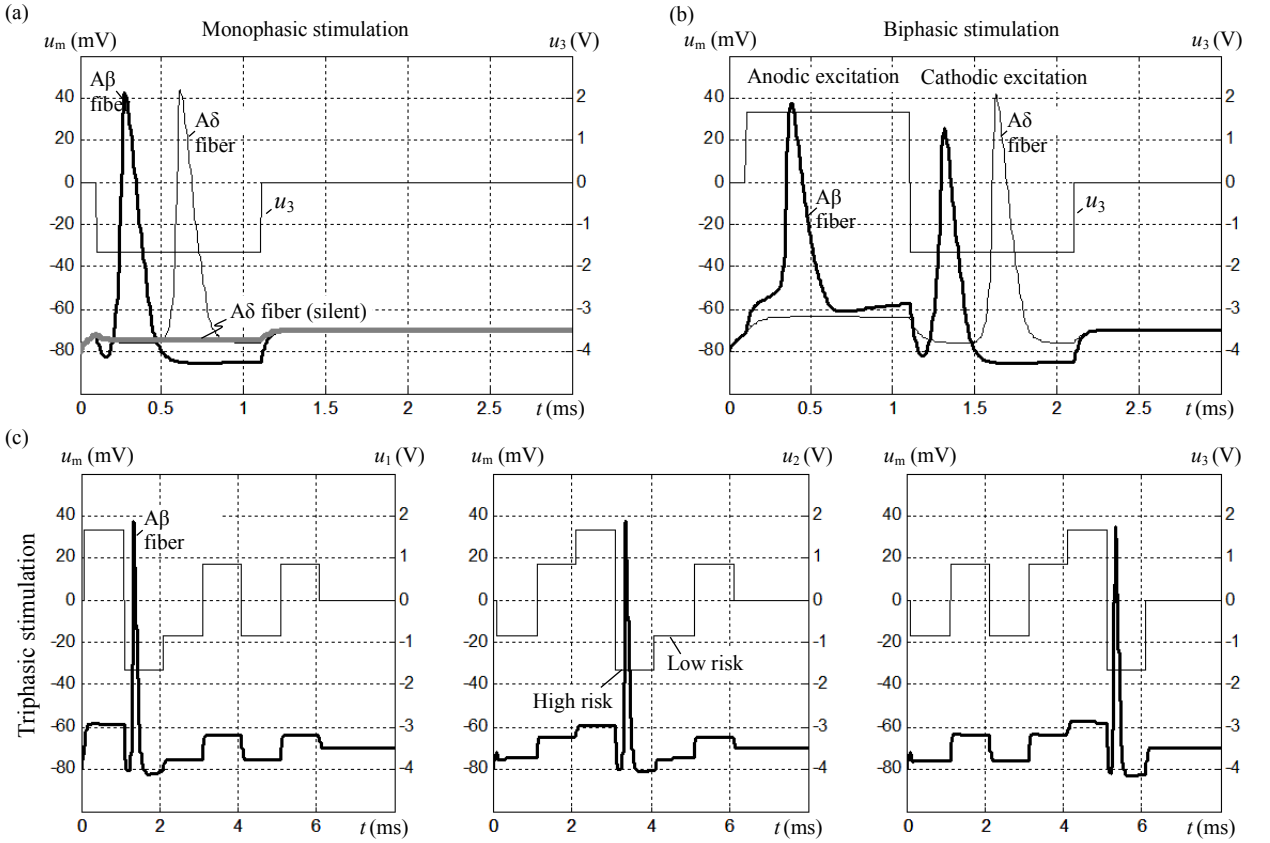

Fig. 6 Excitation of Aβ and Aδ fibers in the individual in-silico model in response to (a) monophasic stimulation at the electrode E_3 of Aβ and Aδ fibers (from the nerve branch (7 Aβ 21 Aδ) in Fig. 1b), (b) biphasic stimulation at E_3 of Aβ and Aδ fibers (from the branch (7 Aβ 21 Aδ) in Fig. 1b), and (c) triphasic stimulation with asynchronous firing of an Aβ fiber at E_1 to E_3 (from branches (22 Aβ 63 Aδ), (11 Aβ 32 Aδ), and (7 Aβ 21 Aδ) in Fig. 1b), all simulated with the burst length $BL = 1$ for the modelled pain threshold level ELc. The time course of the transmembrane voltage u_m (SENN model) is shown along with the applied voltage u_1 to u_3 at E_1 to E_3 (Fig. 1). The risk level for cathodic block of nearby fibers is indicated for two subsequent pulses in TS.

and was qualitatively and subjectively considered as more comfortable than the non-bursted pVNS. No consistent differences in subjective perception were reported between MS, BS, and TS.

Experimenter reported that perceptional resolution of U changes for all stimulation patterns was finer for the bursted stimulation ($BL > 1$) than for the non-bursted ($BL = 1$). Likewise, a smaller change in the absolute U was required to find the different PLs for $BL > 1$, which is in line with the decreased U for $BL > 1$ as compared to $BL = 1$ (Fig. 3).

B. Numerical Data

Numerical peak values U are shown in Table 2 for the individual and simple in-silico models as a function of the stimulation pattern, EL, and the two biophysical neuron models. Values are provided in % as related to the cathodic MS with $BL = 1$ leading to the excitation of at least a single Aβ fiber in the considered model.

As expected, the simulated U increases from ELa, to ELb, and to then ELc (Table 2). Both the non-bursted ($BL = 1$) and bursted ($BL > 1$) stimulations show identical U. The level of U tends to decrease from MS to BS by about 4% in both in-silico ear models and the Sweeney fiber model, whereas a larger decrease of 25% can be observed in the simple model and EL_C. For the SENN model this decrease is much less and amounts to only 0 to 0.6%, again with the exception of the simple model and EL_C showing a decrease of 23%. There is no difference in U between BS and TS, irrespective of the applied in-silico and fiber models.

Table 3 summarizes the relative TN for both in-silico models in comparison with the expected calculated TN (in brackets). For the simple model and $BL = 1$, we get a single action impulse per symbol so that the simulated TN follows the expected TN (= 0.26) for ELb. However, a larger value of 0.67 results than expected 0.63 (= (22+32)/85) for ELc. This value of 0.67 means that 35 Aδ fibers were excited instead of the requested 32 Aδ fibers (50% limit) for ELc. This is due to close vicinity of individual fibers within the model (Fig. 1c) resulting in an almost identical U for the recruitment of 32 or 35 Aδ fibers within the numerical resolution of the model.

For the individual model and $BL = 1$ (Table 3), we see that a share of Aδ fibers were co-excited in addition to all Aβ fibers for ELb; e.g., $TN = 0.4$ means 36 (= (0.4·255)-66) co-excited Aδ fibers. For ELc, values of TN lower than the expected 0.63 (= (66+95)/255) mean that not all Aβ fibers were co-excited together with the requested 95 Aδ fibers (50% limit), whereas TN larger than 0.63 indicates that more than 95 Aδ fibers were excited at the threshold U for ELc due to small inter-fiber distances.

For BS and TS subjected to ELc, more than one action

TABLE 3
SIMPLE AND INDIVIDUAL IN-SILICO PVNS. THE TOTAL NUMBER OF ACTION IMPULSES *TN* IS GIVEN FOR A SINGLE STIMULATION PERIOD $1/f_S$, AS RELATED TO THE TOTAL NUMBER OF FIBERS (NAMELY, 85 FOR THE SIMPLE MODEL AND 255 FOR THE INDIVIDUAL MODEL). TWO DIFFERENT NUMERICAL FIBER MODELS ARE CONSIDERED (SWEENEY / SENN) WHILE FOR IDENTICAL RESULTS A SINGLE VALUE IS PROVIDED. THE EXPECTED CALCULATED VALUE OF *TN* IS GIVEN IN BRACKETS UNDER THE ASSUMPTION THAT A SINGLE ACTION IMPULSE IS GENERATED IN RESPONSE TO EVERY SYMBOL IN MONOPHASIC, BIPHASIC, OR TRIPHASIC STIMULATION.

Burst length *BL*	Excitation level EL	Simple in-silico pVNS			Individual in-silico pVNS		
		Monophasic stimulation MS (1)	Biphasic stimulation BS (1)	Triphasic stimulation TS (1)	Monophasic stimulation MS (1)	Biphasic stimulation BS (1)	Triphasic stimulation TS (1)
1 for MS, BS, TS	ELb	0.26 (0.26)			0.34 / 0.40 (0.26)	0.37 / 0.40 (0.26)	0.37 / 0.40 (0.26)
	ELc	0.67 (0.63)			0.57 / 0.63 (0.63)	0.60 / 0.73 (0.63)	0.70 / 0.80 (0.63)
30 for MS, BS 15 for TS	ELb	7.72 / 7.05 (7.76)	7.72 / 7.69 (7.76)	3.86 / 3.84 (3.88)	9.80 / 9.10 (7.76)	11.20 / 12.10 (7.76)	5.60 / 6.12 (3.88)
	ELc	19.00 / 18.22 (19.06)	19.00 / 18.9 (19.06)	9.50 / 9.45 (9.53)	17.90 / 17.06 (18.94)	18.9 (18.94)	10.50 / 10.60 (9.47)
250 for MS, BS 125 for TS	ELb	64.33/ 58.75 (64.71)	64.33 / 64.08 (64.71)	32.17 / 32.00 (32.35)	81.67 / 75.83 (64.71)	93.32 / 100.8 (64.71)	46.66 / 51.00 (32.35)
	ELc	158.3 / 151.83 (158.82)	158.33 / 157.5 (158.82)	79.16 / 78.75 (79.41)	149.2 / 142.2 (157.84)	157.5 (157.84)	87.50 / 88.34 (78.92)

impulse was observed per single BS or TS symbol, respectively, in some Aβ fibers, as illustrated in Fig. 6b. Thus, multiple impulses per single stimulation period occur for the relatively strong stimulation of Aβ fibers - with lower stimulation threshold than Aδ fibers - and increase the effective value of *TN*.

For the bursted stimulation ($BL > 1$), Table 3 shows that a single action impulse is usually generated with each symbol within bursts since the observed deviations of the simulated *TN* from the expected *TN* are rather small. The absolute deviations increase from the simple model (in the range from -9% to +6% with the median of -0.4%) to the individual in-silico model (from -10% to +58% with the median +17.3%). When the simulated *TN* for ELb is smaller than the associated expected *TN*, it means that not all consecutive symbols within the burst generated individual action impulses. In contrast, higher values of the simulated *TN* for ELb indicate co-excited Aδ fibers. The deviations for ELc are due to still non-excited Aβ fibers, co-excited Aδ fibers (exceeding 50% limit), missing action impulses in response to certain symbols in the burst, and/or multiple action impulses within BS or TS symbols.

IV. DISCUSSION

A. Stimulation Patterns and Electrode Set-up

In MS, a cathodic pulse ($U < 0$, see Fig. 2a) depolarizes the fiber region closest to the extracellular electrode, which, for a straight fiber, has an opening angle of about 70° from the electrode's point of view. The depolarized central region is laterally surrounded by hyperpolarized regions. In contrast, an anodic pulse ($U > 0$) depolarizes lateral regions and yields a strong central hyperpolarization.

In MS with varying polarity, anodic depolarization is weaker by a factor 4 to 8 than cathodic depolarization, whereas the theoretical straight-mode excitation yields the factor 5 [48]. Here the investigated auricular in-silico models have shown factors 1.6-3.7, in line with our previous numerical pVNS data [41]. Therefore, thresholds of cathodic pulses of MS can be assumed to represent the lowest excitation thresholds of the subsequent cathodic and anodic pulses as used in MS (Fig. 2a). Fig. 6b demonstrates a lower threshold of cathodic excitation for the shown Aβ fiber since the cathodic pulse of BS induces an action impulse earlier than the anodic pulse. Cathodic and anodic pulses in MS can be considered to induce independent effects on the fiber's membranes due to a relatively long time in-between these pulses (> 500 ms for maximal $BL = 250$) as compared with the membrane time constant (< 1 ms).

In BS, equally strong depolarizing and hyperpolarizing pulses follow each other so that there is relatively little time for the inert threshold depolarization to develop within a single fiber [32]. Only fibers close to the electrode experiencing strong depolarization stimuli have sufficient time to become excited. In contrast, distant fibers become depolarized and hyperpolarized around their resting state without excitation. This desensitizing effect typically yields larger excitation thresholds for BS than MS, especially for relatively short pulses of about 100 µs (and below). The difference in thresholds progressively disappears with increasing duration of pulses and is already absent for the relatively long pulses of 1 ms, as used in the present study ($t_P = 1$ ms in Fig. 2). These long pulses can be expected to provide sufficient time for the relatively thick fibers of about 10 µm up to the depth of 1-2 mm (from electrodes) to become depolarized and excited either in the cathodic or anodic pulse of BS symbol [33].

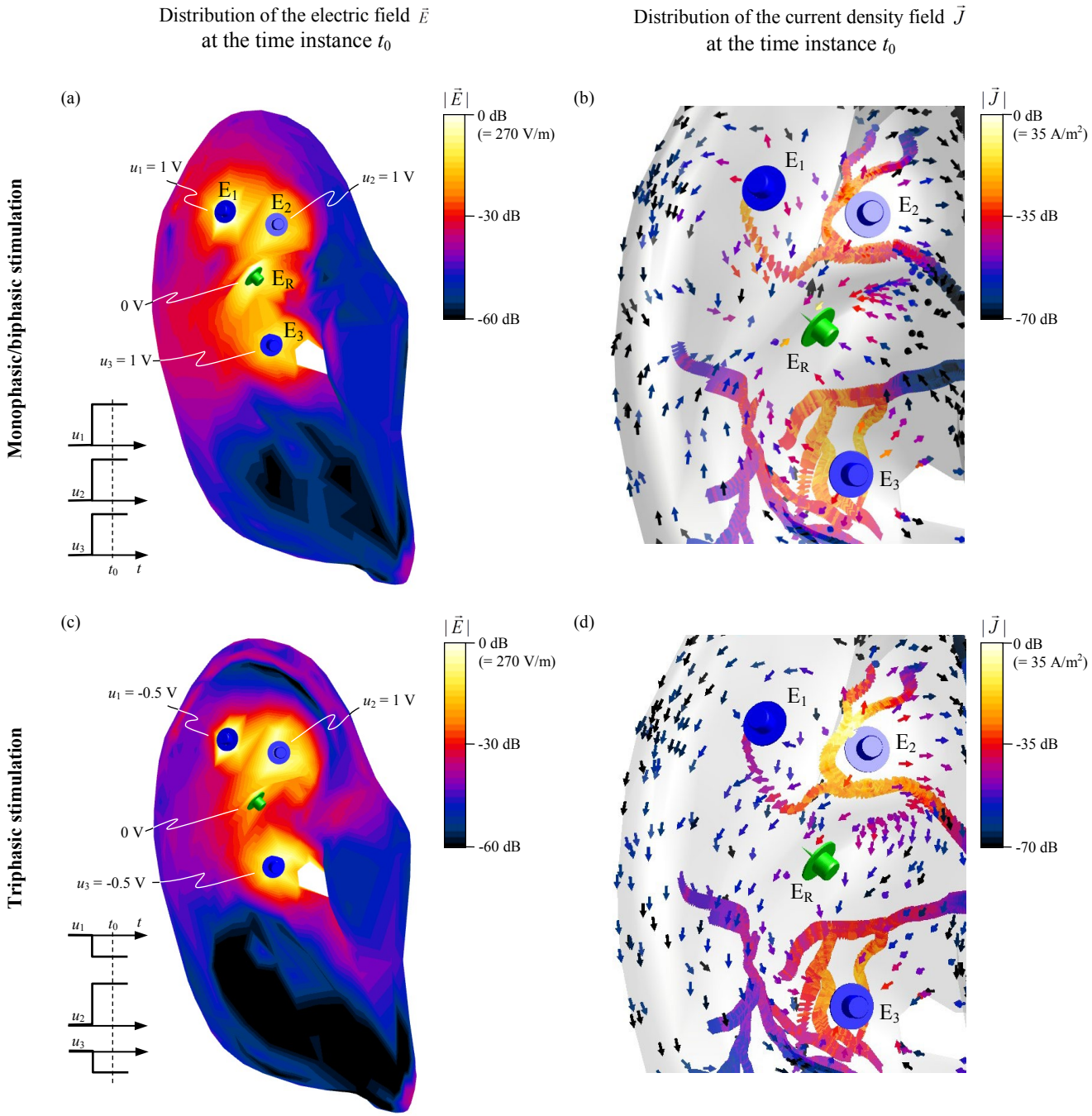

Fig. 7 Distribution of electric and current density fields in the individual in-silico model (Fig. 1b) for the applied electric potentials on electrodes E_1 to E_3 and E_R. a) The magnitude $|\vec{E}|$ of the electric field $\vec{E}$ on the auricular surface at the time instance t_0 for monophasic or biphasic stimulation set-up from Fig. 2a,b, with the dB color scale being linear. b) The associated vectors of the conductive current density field $\vec{J}$ and their magnitudes $|\vec{J}|$. While E_1 to E_3 act as current sources, E_R acts as sink. c,d) $\vec{E}$ and $\vec{J}$ at the time instance t_0 for triphasic stimulation set-up from Fig. 2c (comparable with the time point t = 2.5 ms from Fig. 6c). While E_2 acts as a current source, E_1 and E_3 act as current sinks, and E_R is unloaded.

In BS, the recruitment volume under stimulation electrodes can be expected to be larger for a single BS symbol than for a MS symbol of the same U and pulse duration, especially for longer pulses. This is because disjoint and dense fiber populations under electrodes may experience successive depolarizing cathodic and anodic stimuli within a single phase reversal, i.e., within a single BS symbol. The reversal may yield excited regions at different locations along axons that enlarges the recruitment volume in comparison with a single excited region following a single MS symbol. The reversal enhances also the recruitment of disjoint fibers under electrodes subjected to end-mode or bend-mode excitation [32]. Namely, a monopolar MS symbol may lead either to depolarization or hyperpolarization of an exposed terminus or a bend region depending on its spatial orientation under the electrode. In contrast, the reversal within BS symbol may lead

to depolarization irrespective of the fiber's orientation. Therefore, the different PLs in BS can be expected to be lower than in MS, as supported by results in Fig. 3.

In the novel stimulation mode TS, successive depolarizing and hyperpolarizing pulses have different magnitudes (resembling a triphasic power supply network, see Fig. 2c) so that a weak hyperpolarization will not potentially abolish excitation of distant fibers in response to preceding or subsequent strong depolarization. There will be more time for excitation to be developed on average. In addition, multiple pulses with varying depolarizing magnitudes within a single TS symbol imply that if a nearby fiber experiences cathodic block at a particular pulse, preceding or subsequent pulses of lower magnitudes may circumvent this block and still release an action impulse within the TS symbol. Here cathodic block refers to strong central depolarization accompanied by strong lateral hyperpolarizations, abolishing propagating action impulses generated in the central region [33]. Fig. 6c indicates qualitative risk levels of cathodic block. In fact, the missing block in TS would enlarge the excited region below each electrode and thus is a favorable property as compared with MS and BS. Therefore, the different PLs in TS can be expected to be lower than in BS, as supported by results in Fig. 3.

The proposed tripolar set-up uses three active electrodes E_1 to E_3 (Fig. 1). Tripolar stimulation has been shown to provide more focused, spatially selective stimulation than bipolar stimulation but at the cost of the local stimulation strength [33], [49]. This is valid for electrodes residing relatively close to each other in the distance in the order of the fiber's distance to the electrode, so that activating functions of individual electrodes can constructively or destructively interfere [48]. However, this interference cannot be anticipated to occur in the analyzed pVNS set-up (Fig. 1) because E_1 to E_3 and E_R reside in the mutual distance of 10-15 mm, which is much larger than the expected distance from any electrode to the closest fiber of < 1-2 mm. Fig. 7a,c confirms the absence of interference. Here the strongest electric fields and their excitatory gradients arise only within relatively small regions around electrodes in the radial distance r up to a few millimeters, as governed by the electrical point effect, a strong decrease of the electrical field with $1/r^2$, and an even stronger decrease of the amplitude of the activating function with $1/r^3$ determining the local excitation [33], [50]. Therefore, these regions only insignificantly overlap in space in-between individual electrodes and thus only very little interfere with each other. In line with [50], a distant electrode with its r about three times of r of another near electrode can be neglected. Consequently, excitation of fibers can only be expected near active electrodes while excitation effects of individual electrodes are independent from other electrodes.

The combination of the novel TS with the tripolar set-up (Fig. 1) shows favorable properties. Because the sum voltage acting on the stimulating electrodes E_1 to E_3 is zero at any time (Fig. 2c), it favorably unloads the reference current i_R^T towards zero (to be precise, $i_R^T = 0$ only for symmetrical loads of E_1 to E_3) along the reference E_R. This is in clear contrast to MS or BS where i_R^M or i_R^B along E_R, respectively, accumulates all other stimulating currents from E_1 to E_3 (Fig. 2a,b).

Fig. 7b illustrates the distribution of the conductive current density field in the auricle in MS or BS, indicating that E_R (green) acts as a sink of all currents coming from E_1 to E_3 (blue). In TS, Fig. 7d illustrates that E_R is unloaded while E_2 acts as a source, and both E_1, E_3 as sinks. In particular, the current unloading can also be seen by comparing Fig. 7a with Fig. 7c in that the electrical field strength in the region of E_R is lower in TS than in MS or BS (the local strength is still non-zero due to the electrical point effect [33]).

Therefore, TS avoids the risk of a local over-stimulation with i_R under the electrode E_R. Obviously, performing MS or BS with E_1 to E_3 in succession would also unload E_R that warrants further investigations. In addition, a potential drop-off of any electrode including E_R in TS does not effectively stop pVNS that renders TS more robust than MS or BS where E_R is indispensable.

It should be noted that the stimulated auricular regions (Fig. 1a) are differently innervated by the vagus nerve. The vagus nerve was found in 100% of cases in cymba concha [4] (cc in Fig. 1a) with the associated maximum activation of vagal projections to the nucleus of the solitary tract (NTS) - the termination site of the afferent vagus nerve [10] - during its stimulation, as compared to other auricular regions [51]. Cavity of concha and crura of antihelix (c and ca in Fig. 1a) were found to be partly but non-exclusively innervated by the vagus nerve in 45 and 9% of cases, respectively. However, there is still some controversy on the true anatomical location of the vagus nerve in the ear [52].

pVNS may concomitantly stimulate a few more auricular nerves in addition to the vagus nerve, especially the great auricular nerve (with connections to the spinal cord) or the auriculotemporal nerve (connecting to the nucleus spinalis of the trigeminal nerve). For instance, tracing of the transcutaneous stimulation at the tragus in rats labeled the dorsal horn of the cervical spinal cord, with only sparse labelling of NTS [53]. It is suggested that the tragus stimulation can indirectly influence brainstem regions involved in the autonomous control via the spinal cord and even suggest an indirect innervation of NTS by recruited auricular vagus nerves via the spinal cord.

B. Experimental Data

The present experimental data show that the bursted stimulation ($BL > 1$) decreases the required peak values U to reach different PL and is even subjectively more comfortable when compared with the non-bursted stimulation ($BL = 1$). This is qualitatively in line with [49] reporting that the perceived intensity of the stimulation usually increases with increasing stimulation rates, and is supported by [32] showing that excitation thresholds decrease with increasing number of oscillation periods within a burst.

The smallest U can be observed in TS, followed by BS and with the largest in MS, with the exception of $BL = 1$ with no significant changes from TS to BS and from TS to MS (Fig.

3). Considering the individual perception only, the bursted TS ($BL > 1$) seems to be the most effective stimulation, whereas the non-bursted MS ($BL = 1$) seems to be the least effective stimulation. The size of U_{eff} necessarily rises with increasing BL and the change from MS to BS to TS (3). The latter change increases energy demand needed to power phase reversals with a single symbol (Fig. 2). A single BS or TS symbol requires two and three times, respectively, more power than a single MS symbol for a given U and BL (2). Consequently, U_{eff} of the BS or TS symbol is larger by $\sqrt{2}$ and $\sqrt{3}$, respectively, than of the MS symbol (3). Therefore, the observed perception-related differences in U between MS, BS and TS (Fig. 3) clearly weaken when considering the energy-related U_{eff} (Fig. 4).

While the peak value U is a measure of the nerve stimulation and determines the electrochemical stress at the electrode/tissue boundary, the effective U_{eff} determines the applied metabolic stress on the auricular nerves, the local heat deposition, and the power consumption of the stimulation unit (and determines e.g., the battery size in portable applications). In particular, the metabolic stress is proportional to the applied electric charge per anodic or cathodic pulse, and implies that an overly strong and/or extended pVNS may render neurons less responsive with elevated excitation thresholds up to depressed and refractory [33].

Therefore, while the change of the non-bursted stimulation to bursted stimulation advantageously lowers U, the associated electrochemical stress, and increases the stimulation comfort - in order to reach a certain PL (Fig. 3) - this change disadvantageously raises U_{eff} (3) as well as the power consumption and metabolic stress. However, the demonstrated comparison in-between the analyzed stimulation patterns MS, BS, and TS shows that TS with $BL > 1$ exhibits the lowest levels of U, where there is no difference in U between $BL = 15$ and $BL = 125$ of TS (Fig. 3). Therefore, in line with (3), the setting with TS and $BL = 15$ seems to be energetically in favor over $BL = 125$ (> 15) in terms of a lowered U_{eff}. Fig. 4 confirms experimentally this preference considering not only the energetic but also perceptional aspects. Namely, for all PLs, the required U_{eff} for TS and $BL = 15$ is still significantly lower than for MS and BS with $BL > 1$ (not shown in Fig. 4). In conclusion, the bursted TS with $BL = 15$ seems to be the best compromise for pVNS from perceptional, electrochemical, metabolic, heat, and energetic points of view.

The comparisons between males and females as well as age < 40 and age ≥ 40 disclose only some tendencies in view of the limited data set (Fig. 5). Females tend to be more sensitive to comfortable perception, i.e., females may perceive an increasing U earlier than males, whereas the reverse is true for pain perception, i.e., females may bear a larger U before sensation of intolerable pain. In general, females act more sensitive to electrical stimulation (from perception to pain) and show lower pressure thresholds by about 30% than males [54], which may indicate a higher sensitivity of Aβ receptors in females.

These gender-related differences may be related to different counts of auricular fibers of the vagus nerve. As shown in an anatomical dissection study [37], the median count for Aβ fibers was 95 (in the range 21-108) and 58 (23-133) for 6 female and 12 male ears, respectively, whereas the associated median numbers of the total count of myelinated fibers showed also gender-related differences with 466 (183-548) and 396 (180-544). These insignificant larger numbers for female than male may have contributed to the observed larger sensitivities in females. Other contributing factors are potential differences in neuronal pathways recruited by pVNS, in neuronal sensitivity, and in levels of reactivity of certain brain nuclei, as well as neurohormonal differences between male and female that require further investigations [55].

Younger volunteers show lower U for all stimulation patterns irrespective of BL; in particular, adult volunteers seem to have higher thresholds of pain. The age-related differences may also be related to the different counts of auricular fibers. Anatomical data in [37] and our regression analysis show that the number of Aβ fibers decreases with age by about 1 fiber per ear and per year while the number of the total myelinated fibers decreases by about 5 fibers per ear and per year. However, these decrease rates apply only for elderly population within the age 50 to 96 years (with the median of 72 years). In addition, the number of Aβ fibers was lower for donors with history of diabetes and age >80 years, which is also in line with other reports [56], [57].

These tendencies over gender and age - especially applicable for the comfortable perception PLb as recommended and used for pVNS therapy - may stress the necessity of adaptive and individualized settings of pVNS stimulation parameters.

The current peak values delivered to the body per active electrode and for the perception levels PLa, PLb, and PLc can be estimated to be in the range 0.02-0.6 mA (with the median of 0.2 mA), 0.06-0.9 mA (0.3 mA), 0.08-3.2 mA (0.5 mA), respectively, with the estimated total impedance of the tissue/electrode boundary and the auricular tissue of about 5 kΩ from [33], [58].

C. Numerical Data

The present numerical data show that there is no difference in U for a given EL between the non-bursted ($BL = 1$) and bursted ($BL > 1$) stimulation. We hypothesize that it is due to relatively long pulses of $t_P = 1$ms (Fig. 2). Namely, increasing BL typically decreases the excitation threshold through the rapid non-linear accumulating mechanisms of the membrane excitability [32], [33]. In short, oscillatory stimulus forms progressively a depolarizing bias voltage across the membrane (in the subthreshold range) that favors subsequent excitation and thus lowers its threshold. However, this effect is dominant for relatively short pulses in the range of 100 µs and already disappears for long pulses of 1000 µs - as we have used in the present study - where the rapid membrane excitability cannot accumulate from one long pulse to another for $BL > 1$.

There is only a small change in U from MS to BS, with a noteworthy exceptional decrease of more than 20% for the simple model and EL_C. There is no change in U from BS to

TS, neither in the individual nor in the simple model. This approximate match in *U* for MS, BS, and TS seems to be due to the absence of the desensitizing effect of hyperpolarizing pulses in BS and TS for relatively long pulses of 1 ms as well as the effective absence of rapid accumulating mechanisms of the membrane excitability in neuronal models.

Analysis of *TN* shows that we usually end up with a single action impulse per symbol (Fig. 6a) since the constituting pulses of 1 ms are relatively long and thus can be considered to act independently from other pulses. The particular time stamp of the induced impulse depends on the recruited fibers distance from the electrode, the fiber type, the stimulus type, and other properties. For instance, an Aβ fiber is excited earlier than an Aδ fiber in Fig. 6a since an Aβ fiber is thicker and thus more easily excitable. Even a few subsequent action impulses can result per single symbol for the relatively strong BS and TS acting on easily excitable Aβ fibers (Fig. 6b) that increases the net information flow to the brain. While MS and BS generate almost synchronous impulses at each electrode E_1 to E_3, TS generates asynchronous impulses in fibers located at E_1 to E_3 (Fig. 6c). Thus, TS incorporates three active sites working in sequence with each other, leading to increased asynchronous information flow to the brain and thereby increased efficiency of pVNS. The number of non-overlapping impulses in TS per stimulation symbol is ideally tripled, as compared to MS or BS.

In order to examine the robustness of the simple in-silico model, a simple sensitivity study was additionally performed. Here the distance between the stimulation electrode E_1 and the reference electrode E_R was reduced from 20 mm to 10 mm (Fig. 1c). As the absolute thresholds decreased by about 8%, the reported relative thresholds from Table 2 were subjected to an even smaller change in the range of up to about 2%. Concerning *TN* from Table 3, the reduced distance yielded changes by up to 0.2% only for $BL > 1$ and the SENN model. These sensitivity-related results prove that the simple model is quite robust with respect to the distance between electrodes (Fig. 1c), a relevant boundary condition of the simple in-silico model for pVNS.

D. Experimental versus Numerical Data

Comparison of experimental and numerical data is not straightforward. Experimental data account for both the peripheral stimulation in the ear and the subsequent central processing of the pVNS-generated sensorial information in the brain, in terms of the registered perception levels PL. In contrast, numerical data consider only peripheral stimulation in terms of the registered excitation levels EL.

However, since ELb models cutaneous mechanoreceptive and touch sensation of the ear with the required recruitment of Aβ fibers, this numerical ELb can be assumed to be qualitatively comparable with the experimental PLb accounting for the comfortable perception. Likewise, ELc models cutaneous pain sensation of the ear while recruiting Aδ fibers; ELc can thus be assumed to be comparable with PLc accounting for painful perception. However, percentages of fibers activated at each PL may be questioned.

In particular, comparison between non-bursted ($BL = 1$) versus bursted ($BL > 1$) stimulation shows that while experimental data show clear differences in *U*, numerical data does not. While MS, BS, and TS show significant differences in experimental data, numerical data show only little (MS versus BS) or even no differences (BS versus TS). It can be hypothesized that these experimental differences are due to central processing of the perception in the brain, as assessed in the experiment but not in the numerical simulation.

Experimental thresholds show that the bursted TS seems to be the best option while numerical thresholds do not offer any preference. However, detailed numerical analysis on the level of individual action impulses reveal that TS in combination with the used tripolar electrode set-up generates asynchronous impulses per stimulation symbol in the ear and thus might favorably increase sensorial input to the brain.

E. Limitations

Study limitations include low number of volunteers who, in addition, were healthy and relatively young, thus not representing typical pVNS patients, aged and with chronic complaints. Since needles were removed after each measurement session and the ear was changed in-between sessions, the auricular position of needles showed intra-subject and inter-subject variability. As reviewed by our group [10], the stimulation of the left or right ear cannot be expected to yield different physiological effects since afferent information from both sides are centrally merged in the brainstem [59], and the right and left aVN show comparable counts of Aβ fibers (on average 64 and 78 on the left and right, respectively) [37]. Even though stimulation patterns were permutated from session to session, in each session the size of *BL* was increased over time, which may have influenced the recorded *U* as a function of PL. The duration of sessions ranged from 1 to 2 hours, which was quite long and exhaustive to study participants and thus may have influenced the PL-related *U* at the end of sessions. The comparisons of males versus females as well as of subgroups of different age are strongly limited by small and differently sized data sets.

The interface between needle electrodes and tissue is subject to changes over time that affect the applied stimulation strength within auricular tissue, given the voltage-controlled stimulation. These changes occur with a time constant of a few hours to several days concerning adhesion, migration, and differentiation of cells at the interface [60]. In order to minimize this time-dependent factor, needle electrodes were replaced before each measurement session with its maximum duration of up to 2 hours.

In the numerical study, electrode interface effects were not modeled. In fact, needle electrodes, i.e., polarizable electrodes, act as high-pass filters and thus influence the electric field distribution in tissue and the resulting neuronal stimulation. Please note that the discussed advantageous properties of TS in combination with the tripolar set-up disappear in the simple model where only a single stimulation electrode is used (Fig. 1c). Therefore, TS stimulation becomes more similar to BS in the simple model than in the individual model, which may

have affected the comparison of the different stimulation patterns in these in-silico models.

It should be noted that the potential advantage of TS with the tripled number of action impulses per stimulation symbol holds only for the stimulation of nerves quite near to the electrodes or to the surface of the skin, as compared with the distance in-between electrodes. Otherwise, the independent action of individual electrodes is lost and then the mentioned interference phenomena would determine the excitation of fibers [48].

While the composition of individual bursts in BS and TS does not change from one burst to the next (Fig. 2b,c), the cathodic burst follows the anodic burst and vice versa with the rate f_S in MS (Fig. 2a). Since cathodic and anodic stimulation have different excitation effects - as discussed above - it can be expected that the burst-related excitation effects in MS oscillate with $f_S/2$ while those in BS and TS with f_S. In addition, MS, BS, and TS inject different amounts of the electric charge per symbol and per time unit. Both issues may potentially affect the comparison between all three investigated stimulation patterns and will be addressed in future studies.

The voltage-controlled pVNS does not provide a direct control over the electric charge that is injected into the auricle like the current-controlled stimulation. In addition, a relatively high impedance for one or more electrodes may reduce the resulting stimulation current and thus affect the likelihood of the auricular nerve excitation. However, the selected voltage-controlled stimulation increases the required robustness of pVNS in that a temporal drop-off of electrodes or a loss of the electrode contact (e.g., due to movements) would not shock or induce unexpected pain in subjects. Otherwise, the current-controlled pVNS and quickly deteriorated electrode contact would necessarily and abruptly raise the stimulation strength.

V. Conclusion

pVNS gains importance as a tool in the bioelectronic medicine with the potential to address diverse chronic ailments. It is imperative to move from an empirical selection of stimulation patterns towards efficient and optimized settings.

The present study evaluates the pre-clinical efficiency of different stimulation patterns in pVNS - with respect to perception levels - and compares it with the numerical efficiency of the same patterns - with respect to excitation levels. While experimental data were attained in healthy volunteers, numerical data were based on developed in-silico electromagnetic models of the ear including functionalized axons of the auricular vagus nerve.

The comparison favors the novel TS pattern in combination with the used tripolar electrode set-up. It is instructive to observe that the presented experimental and numerical analysis separates excitatory pVNS effects in the auricular periphery, as accounted by in-silico data and local excitation levels, from the combination of peripheral and central pVNS effects in the brain, as accounted by experimental data and global perception levels.

The innovation of the study is that - for the first time - coordinated experimental and numerical data were used to optimize stimulation patterns of the investigated minimally-invasive neuromodulation, namely pVNS. Moreover, it can be expected that the observed efficiency of stimulation patterns is also applicable for non-invasive and invasive neuromodulation of peripheral nerve endings when using multiple stimulation electrodes.

The present study warrants further in-silico and in-vivo research on pVNS. While the former should focus on optimization of local excitation effects and minimization of energetic footprints of stimulation patterns, the latter should investigate brain-induced clinical effects. Furthermore, neurophysiological studies are needed on the brain level to validate the different stimulation patterns using, for instance, functional magnetic resonance imaging to assess brain activation patterns and/or magnetoencephalography to assess brainstem potentials.

Acknowledgment

The authors gratefully acknowledge all study subjects for their participation and patience during measurements.

References

[1] D. Guiraud, D. Andreu, S. Bonnet, G. Carrault, P. Couderc, A. Hagege, C. Henry, A. Hernandez, N. Karam, V. Le Rolle, P. Mabo, P. Maciejasz, C.-H. Malbert, E. Marijon, S. Maubert, C. Picq, O. Rossel, and J.-L. Bonnet, “Vagus nerve stimulation: state of the art of stimulation and recording strategies to address autonomic function neuromodulation.,” *J Neural Eng*, vol. 13, no. 4, pp. 1–21, Jun. 2016.

[2] J. P. Beekwilder and T. Beems, “Overview of the clinical applications of vagus nerve stimulation.,” *J Clin Neurophysiol*, vol. 27, no. 2, pp. 130–138, May 2010.

[3] J. Ellrich, “Transcutaneous vagus nerve stimulation,” *European Neurological Review*, vol. 6, no. 4, pp. 254–256, Jan. 2011.

[4] E. T. Peuker and T. J. Filler, “The nerve supply of the human auricle.,” *Clin Anat*, vol. 15, no. 1, pp. 35–37, Feb. 2002.

[5] S. Kampusch, E. Kaniusas, and C. Szeles, “New approaches in multi-punctual percutaneous stimulation of the auricular vagus nerve,” *2013 6th International IEEE/EMBS Conference on Neural Engineering (NER)*, vol. 45, no. 10, pp. 263–266, Jan. 2013.

[6] E. Ben-Menachem, D. Revesz, B. J. Simon, and S. Silberstein, “Surgically implanted and non-invasive vagus nerve stimulation: a review of efficacy, safety and tolerability.,” *Eur J Neurol*, vol. 22, no. 9, pp. 1260–1268, Jan. 2015.

[7] E. Kaniusas, S. Kampusch, M. Tittgemeyer, F. Panetsos, R. F. Gines, M. Papa, A. Kiss, B. Podesser, A. M. Cassara, E. Tanghe, A. M. Samoudi, T. Tarnaud, W. Joseph, V. Marozas, A. Lukosevicius, N. Istuk, S. Lechner, W. Klonowski, G. Varoneckas, J. C. Szeles, and A. Sarolic, "Current Directions in the Auricular Vagus Nerve Stimulation II - an engineering perspective.," *Frontiers in Neuroscience*, vol. 13, no. 772, pp. 1-16, 2019.

[8] S. A. Deuchars, V. K. Lall, J. Clancy, M. Mahadi, A. Murray, L. Peers, and J. Deuchars, “Mechanisms underpinning sympathetic nervous activity and its modulation using transcutaneous vagus nerve stimulation.,” *Exp Physiol*, vol. 103, no. 3, pp. 326–331, Dec. 2017.

[9] E. L. Fallen, M. V. Kamath, G. Tougas, and A. Upton, “Afferent vagal modulation. Clinical studies of visceral sensory input.,” *Auton Neurosci*, vol. 90, no. 1, pp. 35–40, Aug. 2001.

[10] E. Kaniusas, S. Kampusch, M. Tittgemeyer, F. Panetsos, R. F. Gines, M. Papa, A. Kiss, B. Podesser, A.M. Cassara, E. Tanghe, A. M. Samoudi, T. Tarnaud, W. Joseph, V. Marozas, A. Lukosevicius, N. Istuk, A. Sarolic, S. Lechner, W. Klonowski, G. Varoneckas, and J. C. Szeles, "Current Directions in the Auricular Vagus Nerve Stimulation I - a physiological perspective.," *Frontiers in Neuroscience*, vol. 13, no. 854, pp. 1-23, 2019.

[11] T. Kraus, O. Kiess, K. Hosl, P. Terekhin, J. Kornhuber, and C. Forster, "CNS BOLD fMRI effects of sham-controlled transcutaneous electrical nerve stimulation in the left outer auditory canal - a pilot study.," *Brain Stimul*, vol. 6, no. 5, pp. 798–804, Feb. 2013.

[12] R. Babygirija, M. Sood, P. Kannampalli, J. N. Sengupta, and A. Miranda, "Percutaneous electrical nerve field stimulation modulates central pain pathways and attenuates post-inflammatory visceral and somatic hyperalgesia in rats.," *Neuroscience*, vol. 356, pp. 11–21, May 2017.

[13] J. Ellrich and S. Lamp, "Peripheral nerve stimulation inhibits nociceptive processing: an electrophysiological study in healthy volunteers.," *Neuromodulation*, vol. 8, no. 4, pp. 225–232, Oct. 2005.

[14] K. J. Tracey, "Reflex control of immunity," *Nat Rev Immunol*, vol. 9, no. 6, pp. 418–428, 2009.

[15] D. A. Groves and V. J. Brown, "Vagal nerve stimulation: a review of its applications and potential mechanisms that mediate its clinical effects.," *Neurosci Biobehav Rev*, vol. 29, no. 3, pp. 493–500, Apr. 2005.

[16] R. S. Gomolka, S. Kampusch, E. Kaniusas, F. Thürk, J. C. Szeles, and W. Klonowski, "Higuchi Fractal Dimension of Heart Rate Variability During Percutaneous Auricular Vagus Nerve Stimulation in Healthy and Diabetic Subjects.," *Front Physiol*, vol. 9, no. 1162, pp. 1–8, Aug. 2018.

[17] S. Kampusch, F. Thürk, E. Kaniusas, and J. C. Szeles, "Autonomous nervous system modulation by percutaneous auricular vagus nerve stimulation: Multiparametric assessment and implications for clinical use in diabetic foot ulcerations," *2015 IEEE Sensors Applications Symposium (SAS)*, pp. 79–84, 2015.

[18] E. Kaniusas, S. Kampusch, and J. C. Szeles, "Depth profiles of the peripheral blood oxygenation in diabetics and healthy subjects in response to auricular electrical stimulation: Auricular vagus nerve stimulation as a potential treatment for chronic wounds," *2015 IEEE Sensors Applications Symposium (SAS)*, pp. 11–16, 2015.

[19] J. A. Clancy, D. A. Mary, K. K. Witte, J. P. Greenwood, S. A. Deuchars, and J. Deuchars, "Non-invasive vagus nerve stimulation in healthy humans reduces sympathetic nerve activity.," *Brain Stimul*, vol. 7, no. 6, pp. 871–877, Jul. 2014.

[20] S. M. Sator-Katzenschlager, G. Scharbert, S. A. Kozek-Langenecker, J. C. Szeles, G. Finster, A. W. Schiesser, G. Heinze, and H. G. Kress, "The short- and long-term benefit in chronic low back pain through adjuvant electrical versus manual auricular acupuncture.," *Anesth Analg*, vol. 98, no. 5, pp. 1359–1364, Apr. 2004.

[21] V. Napadow, R. R. Edwards, C. M. Cahalan, G. Mensing, S. Greenbaum, A. Valovska, A. Li, J. Kim, Y. Maeda, K. Park, and A. D. Wasan, "Evoked pain analgesia in chronic pelvic pain patients using respiratory-gated auricular vagal afferent nerve stimulation.," *Pain Med*, vol. 13, no. 6, pp. 777–789, May 2012.

[22] S. Bauer, H. Baier, C. Baumgartner, K. Bohlmann, S. Fauser, W. Graf, B. Hillenbrand, M. Hirsch, C. Last, H. Lerche, T. Mayer, A. Schulze-Bonhage, B. J. Steinhoff, Y. Weber, A. Hartlep, F. Rosenow, and H. M. Hamer, "Transcutaneous Vagus Nerve Stimulation (tVNS) for Treatment of Drug-Resistant Epilepsy: A Randomized, Double-Blind Clinical Trial (cMPsE02).," *Brain Stimul*, vol. 9, no. 3, pp. 356–363, Jan. 2016.

[23] R. P. Schukro, C. Heiserer, A. Michalek-Sauberer, A. Gleiss, and S. Sator-Katzenschlager, "The effects of auricular electroacupuncture on obesity in female patients--a prospective randomized placebo-controlled pilot study.," *Complement Ther Med*, vol. 22, no. 1, pp. 21–25, Oct. 2013.

[24] F. Huang, J. Dong, J. Kong, H. Wang, H. Meng, R. B. Spaeth, S. Camhi, X. Liao, X. Li, X. Zhai, S. Li, B. Zhu, and P. Rong, "Effect of transcutaneous auricular vagus nerve stimulation on impaired glucose tolerance: a pilot randomized study.," *BMC Complement Altern Med*, vol. 14, no. 203, pp. 1–8, Jun. 2014.

[25] S. Stavrakis, M. B. Humphrey, B. J. Scherlag, Y. Hu, W. M. Jackman, H. Nakagawa, D. Lockwood, R. Lazzara, and S. S. Po, "Low-level transcutaneous electrical vagus nerve stimulation suppresses atrial fibrillation.," *J Am Coll Cardiol*, vol. 65, no. 9, pp. 867–875, Mar. 2015.

[26] A. Straube, J. Ellrich, O. Eren, B. Blum, and R. Ruscheweyh, "Treatment of chronic migraine with transcutaneous stimulation of the auricular branch of the vagal nerve (auricular t-VNS): a randomized, monocentric clinical trial," *J Headache Pain*, vol. 16, no. 543, pp. 1–9, 2015.

[27] K. Kovacic, K. Hainsworth, M. Sood, G. Chelimsky, R. Unteutsch, M. Nugent, P. Simpson, and A. Miranda, "Neurostimulation for abdominal pain-related functional gastrointestinal disorders in adolescents: a randomised, double-blind, sham-controlled trial.," *Lancet Gastroenterol Hepatol*, vol. 2, no. 10, pp. 727–737, Aug. 2017.

[28] B. W. Badran, O. J. Mithoefer, C. E. Summer, N. T. LaBate, C. E. Glusman, A. W. Badran, W. H. DeVries, P. M. Summers, C. W. Austelle, L. M. McTeague, J. J. Borckardt, and M. S. George, "Short trains of transcutaneous auricular vagus nerve stimulation (taVNS) have parameter-specific effects on heart rate.," *Brain Stimul*, vol. 11, no. 4, pp. 699–708, Apr. 2018.

[29] T. Polak, F. Markulin, A.-C. Ehlis, J. B. M. Langer, T. M. Ringel, and A. J. Fallgatter, "Far field potentials from brain stem after transcutaneous vagus nerve stimulation: optimization of stimulation and recording parameters.," *J Neural Transm (Vienna)*, vol. 116, no. 10, pp. 1237–1242, Sep. 2009.

[30] V. Martlé, K. Peremans, R. Raedt, S. Vermeire, K. Vonck, P. Boon, L. Van Ham, M. Tshamala, J. Caemaert, A. Dobbeleir, L. Duchateau, T. Waelbers, I. Gielen, and S. Bhatti, "Regional brain perfusion changes during standard and microburst vagus nerve stimulation in dogs.," *Epilepsy Res*, vol. 108, no. 4, pp. 616–622, Feb. 2014.

[31] C. Á. Szabó, F. S. Salinas, A. M. Papanastassiou, J. Begnaud, M. Ravan, K. S. Eggleston, R. Shade, C. Lutz, and M. De La Garza, "High-frequency burst vagal nerve simulation therapy in a natural primate model of genetic generalized epilepsy.," *Epilepsy Res*, vol. 138, pp. 46–52, Oct. 2017.

[32] J. P. Reilly and A. M. Diamant, *Electrostimulation: theory, applications, and computational model*. Artech House Publisher, 2011.

[33] E. Kaniusas, *Biomedical Signals and Sensors III: Linking electric biosignals and biomedical sensors*. Springer Publisher, 2019, pp. 1–600.

[34] V. Busch, F. Zeman, A. Heckel, F. Menne, J. Ellrich, and P. Eichhammer, "The effect of transcutaneous vagus nerve stimulation on pain perception--an experimental study.," *Brain Stimul*, vol. 6, no. 2, pp. 202–209, May 2012.

[35] E. R. Kandel, J. H. Schwartz, and T. M. Jessell, *Principles of neural science*. New York: McGraw-Hill, 2000.

[36] A. R. Kothe, *Transcutaneous Vagus Nerve Stimulation - Change of psychometric parameters as a function of different stimulation regions*, Doctoral thesis at the Friedrich-Alexander-University, 2009.

[37] S. Safi, J. Ellrich, and W. Neuhuber, "Myelinated Axons in the Auricular Branch of the Human Vagus Nerve.," *Anat Rec (Hoboken)*, vol. 299, no. 9, pp. 1184–1191, Jul. 2016.

[38] S. Kampusch, E. Kaniusas, and J. C. Szeles, "New approaches in multi-punctual percutaneous stimulation of the auricular vagus nerve.," *6th International IEEE EMBS Conference on Neural Engineering*, pp. 263-266, 2013.

[39] E. Neufeld, D. Szczerba, N. Chavannes, and N. Kuster, "A novel medical image data-based multi-physics simulation platform for computational life sciences.," *Interface Focus*, vol. 3, no. 2, pp. 1–6, Jan. 2014.

[40] B. D. Razlighi, S. Kampusch, S. H. Geyer, H. Le, F. Thürk, S. Brenner, C. Szeles, W. J. Weninger, and E. Kaniusas, "In-Silico Ear Model Based on Episcopic Images for Percutaneous Auricular Vagus Nerve Stimulation," *2018 EMF-Med 1st World Conference on Biomedical Applications of Electromagnetic Fields (EMF-Med)*, pp. 1–2, Jan. 2018.

[41] A. M. Samoudi, S. Kampusch, E. Tanghe, C. Szeles, L. Martens, E. Kaniusas, and W. Joseph, "Numerical modeling of percutaneous auricular vagus nerve stimulation: a realistic 3D model to evaluate sensitivity of neural activation to electrode position.," *Med Biol Eng Comput*, vol. 55, no. 10, pp. 1763–1772, Feb. 2017.

[42] A. M. Samoudi, S. Kampusch, E. Tanghe, C. Szeles, L. Martens, E. Kaniusas, and W. Joseph, "Sensitivity Analysis of a Numerical Model for Percutaneous Auricular Vagus Nerve Stimulation," *Applied Sciences*, vol. 9, no. 3, pp. 540–553, Jan. 2019.

[43] J. D. Sweeney, J. T. Mortimer, and D. Durand, *Modeling of mammalian myelinated nerve for functional neuromuscular stimulation*. Proceedings of the IEEE 9th Annual Conference of the Engineering in Medicine and Biology Society, 1987, pp. 1577–1578.

[44] P. Carmeliet and M. Tessier-Lavigne, "Common mechanisms of nerve and blood vessel wiring.," *Nature*, vol. 436, no. 7048, pp. 193–200, Jul. 2005.

[45] F. Tilotta, B. Lazaroo, M.-H. Laujac, and J.-F. Gaudy, "A study of the vascularization of the auricle by dissection and diaphanization.," *Surg Radiol Anat*, vol. 31, no. 4, pp. 259–265, Nov. 2008.

[46] L. S. Alvord and B. L. Farmer, "Anatomy and orientation of the human external ear.," *Journal of the American Academy of Audiology*, vol. 8, no. 6, pp. 383–390, Jan. 1998.

[47] J. Sandby-Møller, T. Poulsen, and H. C. Wulf, "Epidermal thickness at different body sites: relationship to age, gender, pigmentation, blood content, skin type and smoking habits.," *Acta Derm Venereol*, vol. 83, no. 6, pp. 410–413, Dec. 2003.

[48] F. Rattay, *Electrical nerve stimulation: Theory, experiments and applications*. Springer Publisher, 1990.

[49] J. B. Fallon and P. M. Carter, "Neurobionics: The Biomedical Engineering of Neural Prostheses," in *Wiley Online Library*, no. Principles of recording from and electrical stimulation of neural tissue, R. K. Shepherd, Ed. John Wiley & Sons Publisher, 2016, pp. 89–120.

[50] F. Rattay, "Ways to approximate current-distance relations for electrically stimulated fibers," *J Theor Biol*, vol. 125, pp. 339-349, 1987.

[51] N. Yakunina, S. S. Kim and E. C. Nam, "Optimization of transcutaneous vagus nerve stimulation using functional MRI," *Neuromodulation*, vol. 20, pp. 290-300, 2016.

[52] A. M. Burger and B. Verkuil, "Transcutaneous nerve stimulation via the tragus: are we really stimulating the vagus nerve?." *Brain Stimul.*, vol. 11, pp. 945-946, 2018.

[53] K. M. Mahadi, V. K. Lall, S. A. Deuchars and J. Deuchars, "Cardiovascular autonomic effects of transcutaneous auricular nerve stimulation via the tragus in the rat involve spinal cervical sensory afferent pathways," *Brain Stimul.*, vol. 12, no. 5, pp. 1151-1158, 2019.

[54] J. P. Reilly, *Applied bioelectricity: from electrical stimulation to electropathology*. Springer Publisher, 1998.

[55] M. De Couck, R. Cserjesi, R. Caers, W. P. Zijlstra, D. Widjaja, N. Wolf, O. Luminet, J. Ellrich and Y. Gidron, "Effects of short and prolonged transcutaneous vagus nerve stimulation on heart rate variability in healthy subjects," *Auton Neurosci*, vol. 203, pp. 88-96, 2016.

[56] Y. P. Guo, J. G. McLeod and J. Baverstock, "Pathological changes in the vagus nerve in diabetes and chronic alcoholism, " *J Neurol Neurosurg Psych*, vol. 50, pp. 1449-1453, 1987.

[57] R. S. Tiago, P. A. Pontes and O. Brasil Ode, "Quantitative analysis of myelinic fibers in human laryngeal nerves according to age," *Rev Bras Otorrinolaringol*, vol. 74, pp. 45-52 (2008).

[58] E. Kaniusas, L. Gbaoui, J. C. Szeles, T. Materna, and G. Varoneckas, "Validation of auricular electrostimulation by heart rate variability and blood perfusion: possibilities and restrictions," *Proceedings of Microelectronics Conference*, pp. 180-184, 2008.

[59] M. Chen, L. Yu, F. Ouyang, Q. Liu, Z. Wang, S. Wang, L. Zhou, H. Jiang, and S. Zhou, "The right side or left side of noninvasive transcutaneous vagus nerve stimulation: based on conventional wisdom or scientific evidence?," *Int J Cardiol*, vol. 187, pp. 44-45, 2015.

[60] P. Roach, D. Eglin, K. Rohde, and C. C. Perry, "Modern biomaterials: a review - bulk properties and implications of surface modifications.," *J Mater Sci Mater Med*, vol. 18, no. 7, pp. 1263-1277, 2007.